Simulating morphologies of organic semiconductors by exploiting low-frequency vibrational modes

Alexander R. Smith,[1] Ian R. Thompson,[1] and Alison B. Walker[1, a)]

Department of Physics, University of Bath, Claverton Down, Bath, BA2 7AY, United Kingdom

(Dated: 3 April 2019)

Generating morphologies of amorphous organic materials represents a significant computational challenge and severely limits the size of systems that can be studied. Furthermore, the dynamical evolution of a film at high density occurs on timescales impractical to simulate dynamically, limiting the number of independent states that can be generated. This is a problem in glassy systems as well as protein and polymeric systems. To overcome this problem, we identify rigid sections in molecules and construct an elastic network between them. Using normal mode analysis, we calculate the lowest frequency eigenmodes for the network and displace rigid sections along the low-frequency modes. The system undergoes fast structural relaxation, which allows us to generate many structurally independent approximations to a final atomistic morphology rapidly without force-field parameterization. Using these states as high-density starting configurations, we find equilibrium structures through short molecular dynamics simulations that show close agreement with other atomistic molecular dynamics studies. This method provides a convenient alternative for simulating morphologies of large molecular systems without access to high-performance computing facilities.

[a)]Electronic mail: a.b.walker@bath.ac.uk

I. INTRODUCTION

Organic semiconductor devices are fast becoming commercially competitive with their inorganic counterparts. Benefits such as their electronic (and therefore optical) tuneability and their compatibility with large-scale, low-cost manufacturing processes (particularly solution printing) have given rise to technologies including organic light-emitting diodes (OLEDs), organic thin-film and field-effect transistors (OTFTs and OFETs), and organic photovoltaics (OPV)[1–4]. Both small molecule and polymeric films of crystalline, semi-crystalline, and amorphous structure have all demonstrated significant charge mobilities, in some cases higher than the mobility of amorphous silicon[3,5]. With a wide variety of production processes, a large range of candidate organic compounds, and a multitude of possible structural configurations, predictive computer modelling of morphology and charge-transport characteristics provide an inexpensive platform for the design and testing of new devices.

Computer simulation has been used to produce OPV, OLED, and OFET morphologies in molecular and polymeric systems[4,6–11]. While these studies were able to reproduce accurate structures, investigations are limited by system size. In molecular dynamics (MD) simulations, for instance, the computational demand of calculating trajectories for individual atoms quickly reduces the maximum system size that can be simulated in a reasonable time frame[12]. Simulation times can be reduced by representing clusters of atoms as beads, with pairwise potentials tuned to capture the overall behaviour of the cluster when simulated. In coarse-grained molecular dynamics simulations, the computational cost is greatly reduced and morphologies of up to a million molecules have been used to study organic liquid crystals[13] and polymer-fullerene blends[7,8,10,14]. However, for each coarse-grained simulation interactions between any two particles must be parameterized accurately —a process which requires a substantial amount of work —inhibiting automated studies of a wide-range of materials. Further work is then needed to transform the coarse-grained structures into the atomistic morphologies required for calculating charge transfer rates.

The problem of dynamical simulation is further compounded when a large number of structurally independent morphologies can exist (as is the case in highly-disordered systems) as relaxing the system is a computational challenge at high density[12]. After reaching an equilibrium structure, the time required to obtain a new structurally independent morphology is often much larger than is practical. Particles can become kinetically trapped and systems reach a jammed state, becoming mechanically stable and slowing dynamical evolution[12,15,16]. Furthermore, the

number of MD steps required to find a new morphology also increases with system size[12]. This can make studying the morphological evolution of device-scale systems impractical for researchers without access to high-performance computing facilities.

Slow dynamical motion has also been a significant obstacle in the simulation of proteins. Events such as protein folding and evolution of the active pathway often take place over milliseconds[17–19] but, to ensure accuracy and avoid instabilities, the time step used in dynamical simulations must be on the order of femtoseconds. However, by employing an elastic network model (ENM) and performing normal mode analysis, it is possible to describe the functional motion and large-scale dynamics by following a subset of the low-frequency modes. This comes at the expense of losing information about high-frequency motion, which contributes little to structural changes[20–22].

The low-frequency modes are responsible for the highly collective, long-timescale motion and are known to contribute to structural relaxation in glasses[21,23–26]. By imposing rigid section templates, it has been possible to probe such low-frequency conformational changes in short compute times whilst still retaining the overall molecular structure[18,21]

In this work, we present a Simulation of Atomistic Molecular Structures using an Elastic Network (SAMSEN), a method intended for the rapid generation of structurally independent atomistic configurations of molecular and polymeric systems. This method groups parts of molecules into rigid sections, compresses them to thin film densities and employs normal-mode analysis to create multiple atomistic morphologies.

We demonstrate the method on C_{60} systems at high-density (packing fraction, $\phi = 0.62$), displacing the molecules using a small subset of the low-frequency eigenmodes and observing fast structural relaxation of the system. We proceed to demonstrate the method using N,N'-Di(1-naphthyl)-N,N'-diphenyl-(1,1'-biphenyl)-4,4'-diamine (α–NPD) and phenyl-C_{61}-butyric acid methyl ester (PCBM), two prominent organic semiconductor materials, at their respective thin film densities. The morphologies produced are highly amorphous and comparable to those of other simulation techniques. Outputs from SAMSEN simulations of PCBM are then used as initial configurations for atomistic MD simulations which, immediately after reaching stable temperature and pressure, produce structures that show strong agreement with MD-only simulations. We show that this method will be able to provide the basis for future simulations of organic morphologies as the reduction in computational resources will allow far wider and far larger studies to be performed.

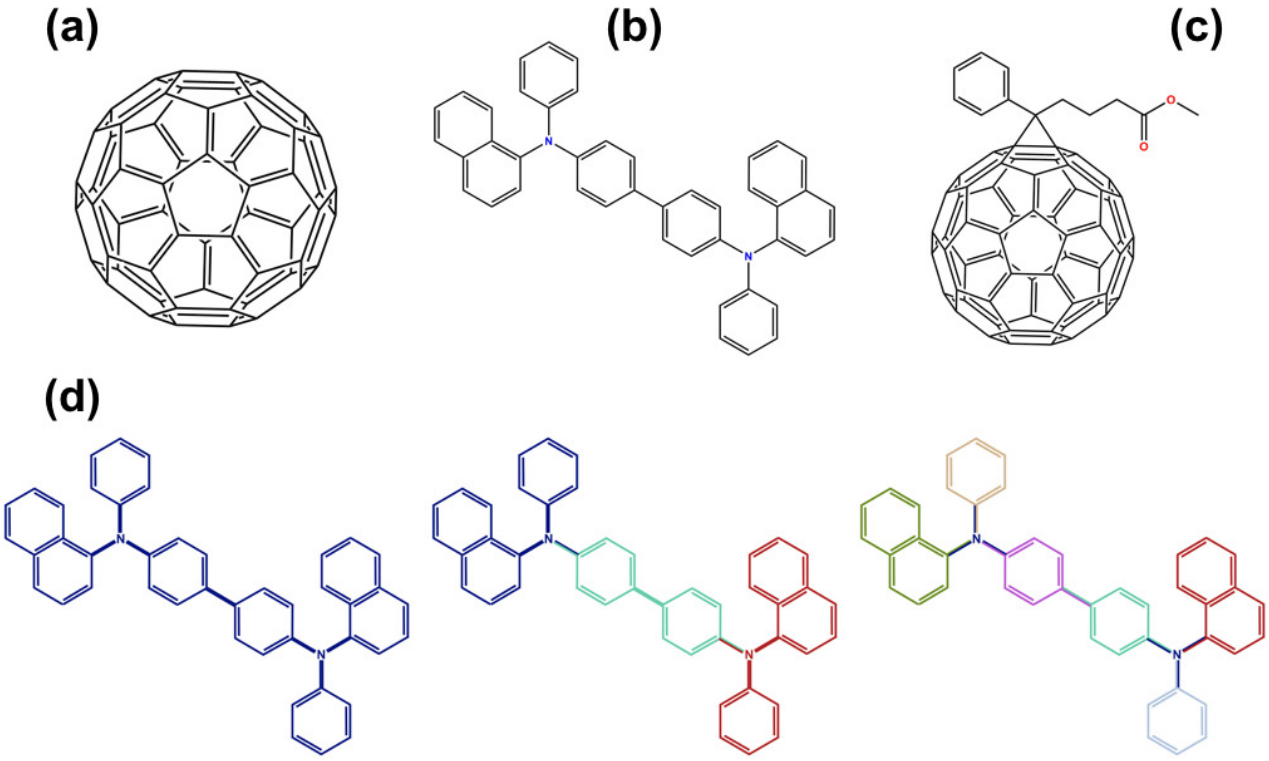

FIG. 1. (a) C_{60} (buckminsterfullerene), (b) α–NPD (N,N'-Di(1-naphthyl)-N,N'-diphenyl-(1,1'-biphenyl)-4,4'-diamine), and (c) PCBM (phenyl-C_{61}-butyric acid methyl ester), the organic semiconducting molecules used in this study. (d) α–NPD is coarsened into varying numbers of rigid sections (colored). The 8 rigid section (right) is produced using the procedure described in section II A. Each aromatic group forms a rigid section, as well as the nitrogen atoms which connect the side groups and the center of the molecule. The 1 rigid section (left) and 3 rigid section (center) groupings used in section III B are also shown.

II. METHOD

SAMSEN samples morphologies quickly by constraining sections of molecules to be rigid and displacing the sections along the normal modes of an elastic network formed between them. The rigid sections can be described as a series of interlocked templates which replace intramolecular interactions. The procedure to determine which sections are rigid is described in section II A. By displacing the system along its normal modes (section II B), the system is able to relax in short compute times. Through an iterative fitting-collision algorithm (section II C) the relative coordinates within the rigid sections can be maintained and compete with atomic hard sphere constraints. SAMSEN borrows from the procedure of Wells et al.[18,21] and is extended to dense molecular systems.

A. Create Rigid Sections

Molecules are transformed into collections of rigid sections using the procedure presented below. At the beginning of the simulation, a template is made of each rigid section which is unchanged throughout. The templates share atoms with their bonded neighbors. After atoms are displaced, the templates are optimally positioned and rotated to check that the relative atom coordinates within rigid sections are within a defined tolerance (if they are not, all atoms are returned to the new template positions). By repeatedly fitting atoms back to their template, bond lengths and angles between any two connected rigid sections can be maintained throughout the simulation. This provides overall rotational and translational freedom for a molecule but also allows a limited degree of bond-angle flexibility. The rigid sections produced are similar to that of Jacobs et al.[27] if covalent bonds are considered the only constraints.

The procedure for determining which sections of the molecule are grouped together as rigid sections is as follows:

1. All atoms (excluding hydrogen atoms) initially form their own rigid section, centered upon their midpoint.

2. Any other atoms bonded to a given atom are then given membership of its rigid section and vice versa. Atoms can be members of multiple rigid sections.

3. If a double-bond connects any two atoms, then their rigid sections are merged –one section now consists of all member atoms from both sections, whilst the other section is deleted.

4. If a region of the molecule is cyclic, all rigid sections in that region are merged (e.g. benzene would consist of a single rigid section).

5. After completing the previous steps, if any rigid section contains no unique set of member atoms (excluding hydrogen) then that rigid section is merged with the one(s) that fully contains it.

This procedure yields a molecule with rigid groups of atoms that hold the overall structure together, but are effectively connected by pairs of concentric hollow rods which allow rotation about their shared axis. The result of the rigid section breakdown is shown for α–NPD in figure 1(d), which forms eight rigid sections around each functional group (including any atoms bonded to the group). If there is only one shared bond between rigid sections, such as between the aromatic sections and the nitrogen-centered sections of α–NPD, both rigid sections can then rotate freely about their shared axis (unless collisions between excluded volumes occur). However, the extent of flexing and stretching is determined by the fitting mismatch threshold, χ_f, (the distance any

one atom can stray from its rigid section template and effectively the difference in radius of two hollow rods) applied universally to all atoms in each rigid section across every molecule.

B. Form the elastic network

Atoms are displaced by low-frequency normal modes, calculated from an elastic network of local contacts between their rigid sections. The ENM used is based upon that of Atilgan et al.[20]. Nodes (rigid sections) are connected by pairwise harmonic potentials of

$$V(r_{ij}) = \frac{1}{2}k(r_{ij} - r_{ij}^0)^2 \tag{1}$$

with an equilibrium length, r_{ij}^0, set equal to the separation, r_{ij}, between nodes, i and j, such that $V(r_{ij}) = 0$. Atilgan et al. used spherical cutoff radii that were system-dependant and tuned, along with the spring constant, k, such that the simulated root mean squared (RMS) displacements matched crystallographic measurements. If the cutoff was too low, there were too many zero-frequency eigenmodes, if too large then the system became too stiff. Requiring a user-specified cutoff radius is undesirable in a general model where, ideally, only nearest neighbors are connected but rigid sections can vary in size and shape. Therefore, to construct the elastic network in SAMSEN, the geometric center of each rigid section forms a node and the network connections (harmonic springs of spring constant, k) are only created if an ellipsoid, enclosing the rigid section, intercepts with another.

These ellipsoids are the minimum volume enclosing ellipsoids (MVEEs) for a section's member atoms, inflated by a small factor, α, calculated before the simulation begins, centrered on the rigid section's geometric center and rotated along with the rigid section template. To determine if two ellipsoids intercept the method of Alfano & Greer[28] is employed. Using ellipsoidal interaction cutoffs assists us in ensuring only nearest neighbor network connections are created, despite the variety of shapes that rigid sections can form. This means there is no need for molecule-specific simulation parameters and a single value of α can be used across all simulations, if the systems are sufficiently dense.

To calculate the normal modes of the system, a $3N \times 3N$ Hessian is constructed (with a 3 $\times$ 3 'super-element' for each pair of rigid sections) where N is the number of rigid sections. If two ellipsoids, belonging to rigid sections i and j, intercept, the corresponding off-diagonal super-elements for those two nodes are populated with the partial second derivatives of the harmonic potential

$$H_{ij} = \begin{bmatrix} \frac{\partial^2 V_{ij}}{\partial x_i \partial x_j} & \frac{\partial^2 V_{ij}}{\partial x_i \partial y_j} & \frac{\partial^2 V_{ij}}{\partial x_i \partial z_j} \\ \frac{\partial^2 V_{ij}}{\partial y_i \partial x_j} & \frac{\partial^2 V_{ij}}{\partial y_i \partial y_j} & \frac{\partial^2 V_{ij}}{\partial y_i \partial z_j} \\ \frac{\partial^2 V_{ij}}{\partial z_i \partial x_j} & \frac{\partial^2 V_{ij}}{\partial z_i \partial y_j} & \frac{\partial^2 V_{ij}}{\partial z_i \partial z_j} \end{bmatrix} \tag{2}$$

where

$$\frac{\partial^2 V}{\partial x_i y_j} = -k \frac{(x_j - x_i)(y_j - y_i)}{r_{ij}^2} \tag{3}$$

The diagonal super-element for rigid section is then filled with elements of the form

$$\frac{\partial^2 V}{\partial x_i \partial y_j} = k \sum_j \frac{(x_j - x_i)(y_j - y_i)}{r_{ij}^2} \tag{4}$$

In this construction, the Hessian matrix is diagonalizable and doing so yields $3N$ eigenvalues, each with an associated three-component eigenvector for each node in the network. If a rigid section forms no contacts with other nodes, then all associated super-elements contain zeros and therefore receive a set of zero displacements across all non-zero frequency modes.

Performing a diagonalization for eigenvalues and eigenvectors can be a computationally-demanding process. To reduce the burden on computer memory, which scales as N^2 and begins to escape the reach of desktop PCs above N = 5000 (using double precision, N = 5000 creates a 1.8 GB Hessian, N = 10,000 uses 7.2 GB), sparse-matrix techniques are utilized. As we are only interested in displacing rigid sections along a small subset containing the lowest frequency eigenmodes, it is possible to speed up the computation by using an Arnoldi iterative shift-and-invert method[29]. This method allows a partial diagonalization to be performed around a chosen central frequency, solving for a specified number of eigenmodes calculated to a set precision.

For large system sizes, solving the eigenproblem using an Arnoldi shift-and-invert method substantially reduces the computation time, taking seconds on a single CPU and less than a second using 8 CPU cores for N = 1000 and 200 modes at high packing. When solving for a small subset of modes, it is also important to set the central frequency such that the lowest-frequency non-trivial eigenmodes are found on the first attempt, otherwise further diagonalizations will be required. To guarantee that the lowest non-zero frequency modes have been found, a check for the presence of zero-frequency translational modes in the partial spectrum is performed.

The low-frequency modes represent collective displacements (minimally changing separations and a low-change in network energy) of nodes (rigid sections) away from a minimum (by construc-

tion). Selecting the low-frequency modes allows us to avoid the highest-energy displacements, where nodes move towards or away from their neighbors. This suppresses the short-timescale movements within nearest neighbor cages and instead focuses on rearrangements over a large-scale. The rigid sections (and molecules) flow[23] through the system whilst the collision-fitting routine maintains the external and internal geometries. The motivation for using this technique is that by utilizing the low-frequency modes, relaxation occurs system-wide in short simulation times as we do not focus on high-frequency movements which do little to relax the structure.

C. The algorithm

To create the initial system, molecules are temporarily assigned MVEEs around all constituent atoms and their ellipsoids are placed in a periodic simulation volume with random positions and orientations, ensuring that no two ellipsoids intercept. Once a starting configuration is found, the ellipsoids are then converted to the atomistic molecules, from which the rigid section groupings and templates are then created. MVEEs are created which enclose and follow each rigid section throughout the simulation and will be used to construct the elastic network.

The system is then compressed athermally to the desired density by scaling all coordinates and box dimensions by a factor, C_f, in steps until the correct simulation dimensions are reached (ensuring collision and fitting conditions are maintained).

The elastic network is then formed between neighboring sections and the diagonalization of the Hessian produces eigenvalues, ω_m^2, and eigenvectors, δ_{im}, for each mode, m, and rigid section, i. The eigenvectors in each mode are then scaled by a factor, β_m, defined as

$$\beta_m^2 = \frac{3k_b\varepsilon}{\omega_m^2\langle\delta_m^2\rangle} \tag{5}$$

where k_b is the Boltzmann constant, and $\langle\delta_m^2\rangle$ is the mean squared displacement of the calculated eigenvectors for each mode, is given by

$$\langle\delta_m^2\rangle = \frac{1}{N}\sum_i^N \delta_{im}^2 \tag{6}$$

and is equal to $1/N$. β_m^2 then represents the RMS displacement of each mode and is determined by ε (which is chosen by the user and becomes the effective temperature for the vibrating system which only supports the chosen number of modes rather than the full $3N$ set) and the eigenvalues and eigenvectors which are a property of the elastic network. If one sets α such that network

connections can only form between nearest neighbors, the displacement of rigid sections in the system is then determined solely through ε and the number of modes selected.

Each rigid section is then assigned a displacement, $\boldsymbol{D}_i$, equal to the sum of their scaled eigenvector across the chosen range of modes, $m_{min} \leq m \leq m_{max}$:

$$\boldsymbol{D}_i = \frac{1}{\sqrt{M_i}} \sum_{m_{min}}^{m_{max}} \beta_m \delta_{im} \tag{7}$$

where M_i is the mass of the rigid section i (here set to 1 atomic mass unit for all sections) and $m = 1$ is the first non-zero frequency eigenmode (this excludes translational modes from the simulation). The range of modes that contributes to $\boldsymbol{D}_i$, for brevity, shall be written $m_{m_{min}}^{m_{max}}$. Every atom is then displaced by the average $\boldsymbol{D}_i$ of the rigid sections that the atom is a member of. The displacement is distributed evenly over S steps so that the procedure maintains steric volume and fitting constraints through use of an iterative collision-fitting routine.

At each step, collision detection is performed to ensure that any two atoms which do not share membership of a common rigid section, do not have overlapping spherical steric volumes. Atoms k and l, not both in the set of atoms A_i which are members of rigid section, i, are considered to have collided if they are separated by a distance, r_{kl}, that is smaller than the sum of their boundary radii, R, less the collision threshold, χ_c:

$$r_{kl} < (R_k + R_l) - \chi_c \qquad k \cap l \nsubseteq A_i \tag{8}$$

Boundary radii are taken from Boyd[30] for all atoms except hydrogen which is set to χ_c. If collisions are observed, all atom pairs where $r_{kl} < (R_k + R_l)$ are then displaced in opposing directions along a vector connecting their centers, such that their boundaries are just touching. If an atom collides with multiple atoms, the mean of the correcting displacements is applied. These collision displacements are executed simultaneously across the system.

Once the collision correction has been applied, the new geometric midpoint of each rigid section is then determined. The corresponding initial template is then centered on the new midpoint and rotated to minimize the total displacement of the atoms from their template. The details of this optimization process are discussed by Wells et al.[31]. After finding the optimal fit, if any atom has coordinates more than a small fitting threshold, χ_f, away from its corresponding template coordinate, then all atoms are moved to the new template positions and the system re-examined for collisions. The collision-detection and fitting routines continue iteratively until both of the user-specified thresholds χ_c and χ_f are met. The collision-fitting routine can be considered a

minimization process, balancing structural constraints with inter-atomic repulsion. After S displacement steps, another SAMSEN cycle begins with the construction of a new elastic network.

The procedure continues until a desired number of cycles have been performed or until fitting and collision conditions cannot be met.

III. SIMULATIONS

The following simulations were performed to demonstrate the applicability of SAMSEN to a wide-variety of molecules in a generalized approach. We study three molecules: C_{60}, α–NPD, PCBM; by compressing systems to film-like densities and comparing the structures to other simulation procedures. The initial structures for these molecules were downloaded from ChemSpider[32] and PCBM was minimized in an OPLS-AA force-field[33]. Parameters $\chi_c = 0.6$ Å, $\chi_f = 0.2$ Å, $M_i = 1$ a.m.u., $k = 1$ kg ps^{-2}, $\alpha = 1.2$, $S = 1000$, $C_f = 0.99995$ are used across all systems studied. Unless otherwise indicated, ε = 200 K and modes m_1^{12} are used for all simulations. Quick structural relaxation of the system is observed for the systems through the self-intermediate scattering function (equation 9), even at high-packing fraction. In this section we also present spectra of the vibrational modes and discuss how we can exploit their distribution to improve sampling performance.

We then study the PCBM system further by taking SAMSEN output states as initial configurations for molecular dynamics simulations. We find SAMSEN states are similar to the conjugant-gradient minimized states and the short- and medium-range structure, exhibited in other MD studies, is then recreated immediately after reaching $T = 300$ K and $P = 1$ atm during NPT simulations.

A. Fullerene

One thousand buckminsterfullerenes (C_{60}), each consisting of one rigid section containing all sixty atoms, were placed at random positions and orientations in a cubic and periodic simulation volume of side 122 Å. The MVEE axis lengths are a = 5.23 Å, b = 5.21 Å, c = 5.17 Å (not quite a sphere). The molecule had an effective radius of 4.25 Å (inferred from the radial distribution function) which accounts for χ_c. The system was then compressed athermally ($\varepsilon = 0$ K), running the collision-fitting routine between each compression, until either the thresholds χ_c and χ_f could no longer be maintained, which occurred at a packing fraction, ϕ = 0.627. We define the packing

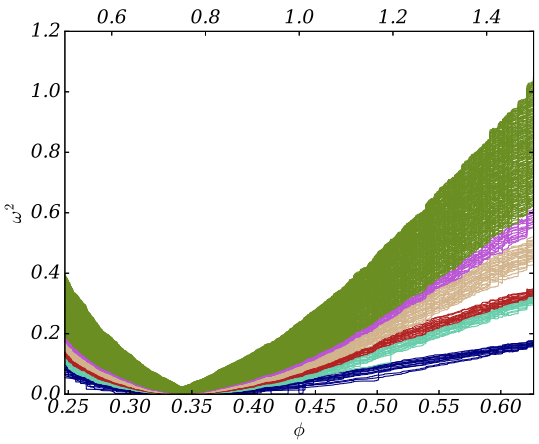

FIG. 2. The lowest 200 eigenvalues (ω^2) for the C_{60} system during compression shown as a line plot against the packing fraction, calculated using the C_{60} effective volume (bottom) and inflated minimum volume enclosing ellipsoid (top). The colors indicate the selections of modes referenced in the text (the lowest 12 modes in each color-band were used in the mode-varying simulations. Zero-frequency (including translational) modes are not shown.

fraction, ϕ, as the ratio of the effective excluded volume (assuming spheres with radius equal to the effective C_{60} radius) to the simulation volume. We also define the ellipsoid packing fraction as the ratio of the total inflated ellipsoid volume to the simulation volume.

Figure 2 shows the vibrational frequencies of the elastic network during compression. At low-densities, the average number of network contacts is relatively small, but the number of contacts (initially) increases linearly with density as the system is compressed. At low packing, the frequencies reduce in value towards zero frequency (the vibrational period diverges) until the average number of contacts reaches 6 (the Maxwell criterion for rigidity of a solid[34]) at $\phi = 0.342$ (ellipsoid packing fraction of 0.75). Zero-frequency non-trivial modes (soft modes) are present, but are not shown, up to this density. These soft modes have been observed in systems of isostatic soft spheres at the jamming threshold when neighbor contacts are removed[16]. Some soft modes are present up to $\phi = 0.44$ where the fewest connections any one node has reaches 4 —the minimum number of contacts required to pin a particle in position[16].

At higher densities, the system is constrained enough by ellipsoid contacts to prevent soft modes from forming. The frequencies begin to increase with increasing density, as the network become stiffer, until at $\phi = 0.47$ (ellipsoid packing fraction of 1.12), where the distribution of frequencies begins to split into five distinct bands of 12 (blue), 24 (aquamarine and red), 22 (tan),

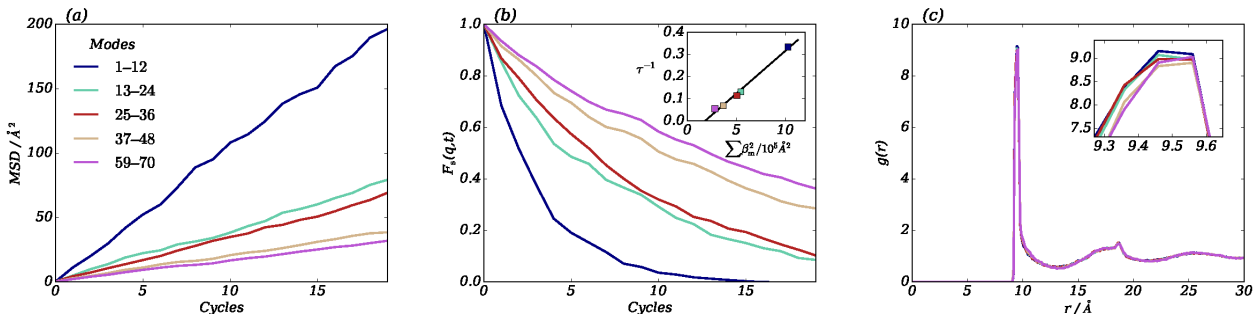

FIG. 3. (a) The mean squared displacement, MSD, (b) the self-intermediate scattering function, $F_s(q,t)$, with $q = 2\pi/9.5Å^{-1}$ and (c) the center-center radial distribution function, $g(r)$, for the C_{60} simulations, displacing the molecules by the lowest 12 modes in each of the four bands at ϕ = 0.62, ε = 200K. The inset of (b) shows a linear dependence of the decay constant (inverse of the relaxation time), τ^{-1} , to the corresponding RMS displacement per cycle. The lowest frequency band (modes 1 to 12) exhibit the fastest motion and relaxation times, with little change to the resulting structure (changes in the peak of $g(r)$ shown in inset of (c)).

12 modes (magenta) as well as the remaining $3N-73$ modes (green). Three global translational modes are also present (but not shown). These bands signify the emergence of and then the separation between the collectiveness of vibrational modes in the system. As we shall show, such a clear distinction between sets of modes can be exploited to preclude computationally-slow high-frequency motion and encourage structural relaxation.

Using the morphology at a molecular packing of $\phi = 0.62$ (as the magenta band begins to emerge), five simulations were performed comparing the displacement of molecules following the lowest 12 modes within each band, as well as the upper half of the second-lowest band (m_1^{12}, m_{13}^{24}, m_{25}^{36}, m_{37}^{48}, m_{59}^{70}), at ε = 200 K for 200 cycles. After an initial increase in frequency and widening of the band gap, the eigenvalues remained approximately constant throughout, but with increasing variance for the higher-frequency simulation.

Using the method presented, molecules were displaced by at least their diameter after ten cycles for the lowest-frequency band, as shown in figure 3a. The largest mean-squared displacements (MSD) were observed in the simulation following the lowest frequency-band of normal modes, reducing markedly across higher bands. Since the molecules are not trapped in local energy minima, the displacement continues at this pace throughout the simulation. The fixed pace of the displacements implies that the motion is diffusive and unhindered by neighbor cages. A similar observation

of a flowing phase at large amplitudes was recently found in a study of disordered systems using active oscillation[23,35].

To measure the structural relaxation across the system we use the self-intermediate scattering function, $F_s(q,t)$, given by

$$F_s(q,t) = \langle \frac{1}{N} \sum_{i}^{N} exp(-iq[r_i(t+t_0) - r_i(t_0)]) \rangle \tag{9}$$

which measures the correlation of particle positions between a state at time t_0 and a later state at time $t+t_0$, probed using Fourier component, q, which directly relates to a characteristic length-scale[36]. In figure 3b, the self-intermediate scattering function is shown for $q = 2\pi/9.5$ Å^{-1} (corresponding to the C_{60} diameter) averaged over 20 cycles. From figure 3b it is most apparent that the lowest frequency-band exhibits the fastest structural relaxation for the system, with the intermediate scattering function falling to zero after 15 cycles. The relaxation time, τ, (when $F_s(q,t)$ falls to $1/e$)[26,35,37] was measured by fitting an exponential decay to these results and was found to be approximately three cycles for the lowest band. The second and third bands are, although less efficient, still able to relax the system at a faster rate than the highest frequency band. In all of these simulations there is the lack of a shoulder in the intermediate scattering function, suggesting that we avoid a two-stage relaxation entirely.

The radial distribution function, $g(r)$, is a commonly used method for characterizing the structure of liquids and is given by

$$g(r) = \frac{V}{N^2} \langle \sum_{i}^{N} \sum_{i \neq j}^{N} \delta(r - r_{ij}) \rangle \tag{10}$$

where δ is the Dirac delta-function and V is the volume of the system. In figure 3c we show $g(r)$ for the simulations displaced by each of the bands. The distributions overlap almost perfectly, with a small difference in height of the nearest neighbor peak (shown in inset) and resembles systems of repulsive monodisperse spheres near jamming[38]. This result is not unexpected, as the molecules are tightly packed and of the same, near spherical, shape.

Both ω^2 and ε determine the RMS displacement in a given cycle, which affects the rate at which independent states are generated. However, the distribution of eigenvectors in each mode (the mode participation) also plays a role. In order to establish that the difference in participation and collective behaviour of the modes was the leading cause of the change in relaxation time (rather than just the shift in frequencies) and to study the effect of changing ε, further simulations

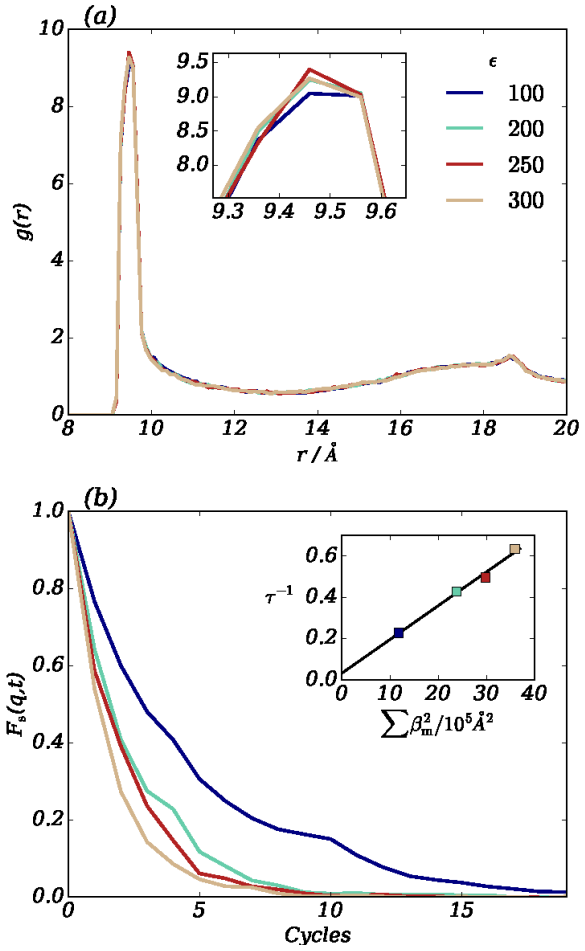

FIG. 4. (a) The radial distribution function (detailed view of nearest neighbor peak in inset) and (b) intermediate scattering function of the C_{60} simulations comparing ε with $q = 2\pi/9.5Å^{-1}$. The inset of (b) can be compared to figure 3(b), both showing a linear dependence of the decay constant (inverse of the relaxation time), τ^1 , of $F_s(q,t)$ upon the total applied RMS displacement.

were performed at the same packing fraction. The C_{60} molecules were displaced using m_1^{24} and four simulations performed with ε set to 100, 200, 250, and 300 K.

We show $g(r)$ for the ε-varying simulations in figure 4a. The overall peak positions and shapes are similar, but there are differences in sharpness of the nearest neighbor peaks (shown in the inset). The remaining features do not change between simulations, however.

In figure 4b, $F_s(q,t)$ is measured as before and the relaxation time, τ, obtained. As would be expected, the larger amplitude displacements lead to faster structural relaxations with τ = 1.6 cycles for ε = 300 K. For decreasing ε, $F_s(q,t)$ decays over increasing timescales.

With a decay constant defined as τ^{-1}, the inset of figure 4b shows τ^{-1} for $F_s(q,t)$ as a func-

tion of the sum of RMS displacement across the selected modes, $\sum \beta_m^2$, for the range of ε studied. This shows a linear dependence with a proportionality constant of 1.63×10^{-7} Å^{-2} cycle^{-1}. Performing the same analysis for the mode-varying simulation (inset figure 3b), the proportionality constant between τ^{-1} and $\sum \beta_m^2$ is twice as large at 3.87×10^{-7} Å^{-2} cycle^{-1}.

The difference between the two gradients shows that, after normalizing for displacement, the collective character of the modes has an impact upon the relaxation time that is stronger than simply increasing particle velocities (increasing system temperature). Comparing the relaxation time for the ε = 200 K simulations using modes m_1^{12} and m_1^{24}, it appears adding more modes is less efficient at relaxing the system per displacement applied (in the limit of a large number of modes, displacements appear random and uncorrelated). Therefore, if one wants to achieve quick structural relaxation, use of the lowest-frequency modes at high amplitude appears to be an efficient method to do so.

It is important to stress that the choice of effective temperature and modes can have a great effect on the computational time required to generate each independent state. Structural relaxations that take place after only one or two cycles, greatly reduce the overall computational demand, especially when the system sizes become large. However, using large amplitudes does increase the number of collisions and demand upon the fitting routine, altering the required computational time per cycle. Lowering the step resolution, S, has a similar effect, particularly for large ε. This is particularly true when rigid sections contain a larger number of atoms —the fitting optimization is performed faster on many smaller bodies than fewer larger ones. Using low frequency modes appears to result in the fewest collisions (for C_{60} at least) and therefore lowers both the time per cycle and cycles per relaxation (the relaxation time) compared to high frequency modes. Balancing these demands can be difficult, however, as we shall see in the next section, reducing the number of rigid sections can also lower the relaxation time.

B. α–NPD

N,N'-Di(1-naphthyl)-N,N'-diphenyl-(1,1'-biphenyl)-4,4'-diamine, or α–NPD, is a widely-studied organic hole-transporting molecule used in OLEDs and OTFTs[11,39,40]. α–NPD layers are generally amorphous, at a density of around 1.15 g/cm^3 (although values in the range of 0.9 to 1.45 g/cm^3 are given) and show only a small preference in their relative orientation[11,39–42]. This molecule is pertinent to our study as the chemical structure (rigid aromatic rings connected by sin-

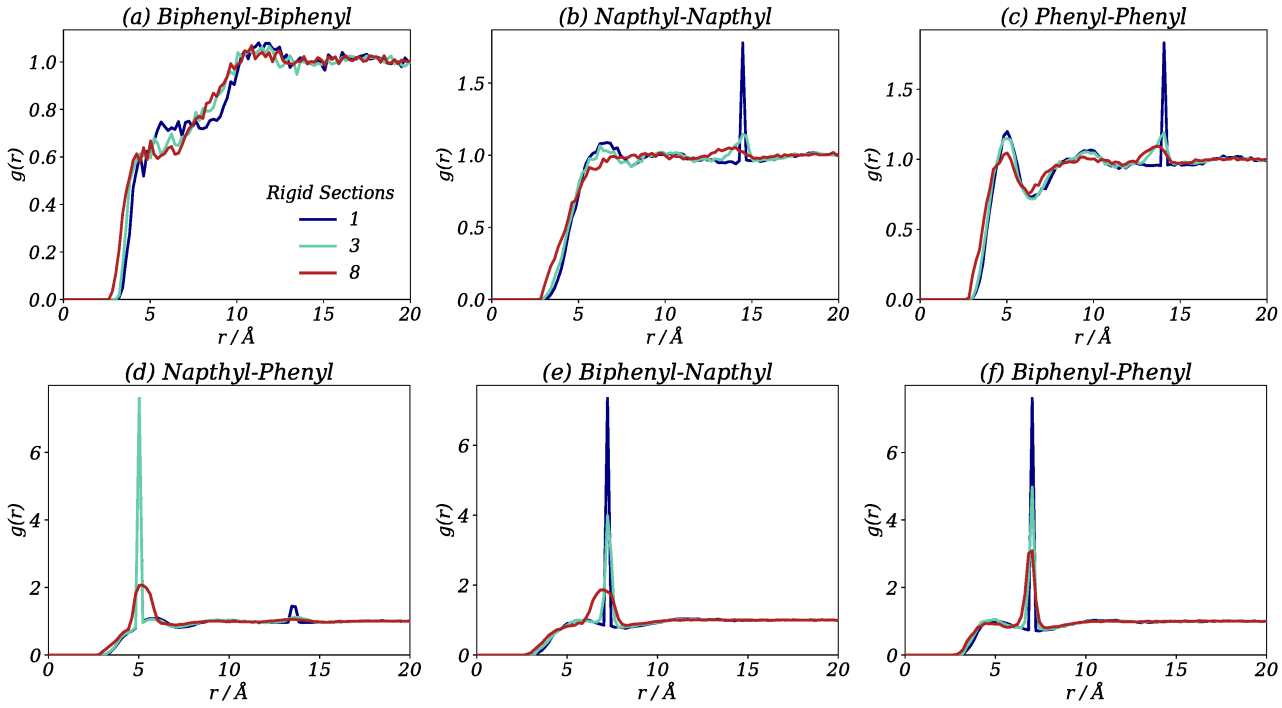

FIG. 5. The radial distribution functions for α–NPD simulations of 1, 3, and 8 rigid sections as measured between the between the average atomic positions of the functional groups. The biphenyl-biphenyl pairing can be assumed to represent the $g(r)$ between the centre of the molecule.

gle bonds as well as two trigonal bonding geometries) allows us to examine how varying numbers of rigid sections affects the local structure and relaxation time during the SAMSEN procedure.

One thousand α–NPD molecules were simulated for the three different rigid section groupings shown in figure 1d. In one simulation the entire α–NPD molecule constituted a single rigid section. In the second, three rigid sections were formed that were joined at the nitrogen atoms. In the final simulation, the method described in section II A was applied and produced an α–NPD molecule with eight rigid sections, consisting of each of the six aromatic groups and a further two centered on the nitrogen atoms. Following compression from a sparse vapour phase down to a film-like density of 1.15 g/cm^3, the rigid sections were displaced using modes m_1^{12}. The radial distribution function was averaged every 10 cycles, excluding the first 10 and measured between the different functional groups of the molecule, with the biphenyl-biphenyl measurement representing the centre-to-centre $g(r)$. The self-intermediate scattering function was then measured for each of the simulations averaged over 30 cycles.

As is apparent from the radial distributions measured between different functional groups of

the molecule in figure 5, SAMSEN produces a dense fluid-like $g(r)$ for all functional groups when each group is given rotational freedom. Each of the simulations produce similar short-range separations between external functional groups and between the molecules as a whole, demonstrated by a minor nearest-neighbor peak between 5 and 6 Å and a second peak at 11 Å in the centre-to-centre (biphenyl-biphenyl) measurement (figure 5a). Interestingly, the fewer rigid sections —therefore the more coarsely-grained the simulation —the more strongly defined the detail produced in $g(r)$ becomes This is particularly true for separations corresponding to the internal structure of the molecule. While there is less detail in the eight rigid section simulation, the first shoulder appears at similar positions, regardless of the number of rigid sections or the functional group the measurement is made from, and the first and second peak (for either the internal or external separations) is always sharpest in the single rigid section simulation.

The reduced structural features shown in $g(r)$ could be due to the additional internal rotational freedom in the many-section α–NPD, which lowers the regularity of separation between the molecular centers (this rotation would usually be limited by dihedral potentials). Setting χ_f to 0.2 Å also permits a large amount of bending when the molecule consists of more rigid sections. This may also explain the broadening of the leading-edge of figure 5a. This is perhaps more likely than attributing the differences in structure to the differing displacements of the vibrational modes. While higher frequency motion is more independent and therefore more likely to cause collisions, little change was noticed in the C_{60} radial distributions when displaced along differing modes.

Observing the change in the peaks in the radial distribution functions corresponding to internal separations, we can observe the effect of increasing internal freedom in the molecule. Looking at the phenyl-phenyl $g(r)$ (figure 5c), the peak at 14 Å corresponds to the separation between the phenyl groups on the opposite side of the molecule. For 1 rigid section, the peak reaches a value of around 1.8. When we switch to the three rigid section simulation, we enable rotation of the ends of the molecule and the peak falls to 1.2. The peaks broaden only to closer (lower) separations because α–NPD is initially in a trans-configuration so separations cannot increase. By then switching to eight rigid sections, we enable the rotation and flexing of the phenyl groups (beyond the simple rotation and bending enabled in the three section simulation, now assumed by the nitrogen-centred rigid sections). This further diminishes the 14 Å peak and it broadens to closer separations. Since the free rotation of the phenyl group is unable increase separations between phenytl groups, the change in separations between three and eight sections is due to the bending and also the distortion of the functional group, controlled by χ_f. This is also the case for

the napthyl-napthyl $g(r)$ in figure 5b.

This perspective is also supported by the napthyl-phenyl $g(r)$ in figure 5d, with the internal peak at 5 Å in the one and three rigid section simulation showing the same amplitude and width. However, the second internal peak at 15 Å corresponding to the far side of the molecule is lost in the three rigid section simulation due to rotation. It is only when you allow bending by going to the eight rigid section simulation that you see any change in the 5Å peak - the napthyl and phenyl groups can now bend both towards and away from each other, being on the same side of the molecule. In the case of the biphenyl to napthyl and biphenyl to phenyl (figures 5e,f) the changes are dominated by bending motion.

Turning to the α–NPD modes, a splitting of the modes into vibrational bands like that of C_{60} was observed. In the range of interest (m_1^{12}), the eight rigid section simulation produces the narrowest vibrational band at the lowest frequencies. The frequencies increase to a value around two times greater for the three rigid section simulation and to a value four to five times greater for the one rigid section simulation. It appears that the larger, more eccentric ellipsoids of the one rigid section α–NPD (with a less uniform set of separations between nodes than the smaller, more regular ellipsoids of the eight rigid section α–NPD) corresponds to an increase in frequencies.

As an increase in frequency represents a reduction in the collectiveness of the modes, one would therefore expect longer structural relaxation times for the single rigid section system. This is evident in the decay of $F_s(q,t)$ using $q = 2\pi/12$ Å^{-1}. For the three simulations, τ reduces for an increasing number of rigid sections, with a relaxation time of 30, 10, and 8 cycles for 1, 3 and 8 rigid sections respectively. This is likely caused by a combination of both differing mode collectiveness and applied displacement. So while a less constrained molecule (more rigid sections) has the least-pronounced structure, it undergoes structural relaxation in the fewest SAMSEN cycles.

C. PCBM

The main aim of this study was to reproduce multiple morphologies of amorphous organic films in short timescales using SAMSEN. We therefore decided to study phenyl-C_{61}-butyric acid methyl ester (PCBM), a popular electron-transporting molecule used in OPV devices, to demonstrate that we can produce a series of morphologies which resemble those of other studies.

Having employed SAMSEN to rapidly generate a series of morphologies at solid-like density (with structural features similar to those of other studies), one could then use more demanding sim-

ulation methods to recreate a more accurate short-range structure. By using SAMSEN generated states as inputs for molecular dynamics simulations, we find that we can recreate the remaining short-range structural details of Cheung et al.[43] and Tummala et al.[10] in as little as 60 picoseconds of total MD simulation time.

As fewer rigid sections captured the most short-range structural details, whilst still allowing the system to relax, we decided to treat PCBM as a single rigid section encompassing the entire molecule. A single molecule was minimized in a vacuum using conjugant-gradient minimization[44] in LAMMPS[45] using the OPLS all-atom[33] force-field of Cheung et al.[43] and used as the template rigid section. A SAMSEN simulation using one thousand PCBM molecules was then performed in a manner similar to α–NPD. The vapour system was compressed to a density of 1.45 g/cm^3, slightly above the density of Cheung et al. (1.44 g/cm^3), and the molecules were displaced using the 12 lowest frequency modes. The relaxation time was measured to be 8 cycles, with $F_s(q,t)$ falling to zero after approximately 30 cycles.

Fifty output states, each separated by 10 cycles, were then used as initial states for LAMMPS molecular dynamics simulations using the same OPLS-AA force-field as Cheung et al.. For each simulation a conjugant-gradient minimization was performed on a SAMSEN state and an NVT simulation (Nosé-Hoover thermostat[46,47]) followed to heat the simulation volume to 300 K over a period of 50 ps. This was then followed by an NPT simulation (anisotropic barostat) to stabilize the pressure at 1 atm, requiring approximately 10 ps, with the density decreasing slightly to 1.446 $\pm$ 0.002 g/cm^3. This MD procedure took an average of 90 minutes to perform on 24 CPUs (36 CPU hours) and SAMSEN took an average of 6 CPU hours to generate each independent state.

Figure 6 presents a comparison of the radial distribution functions for the center-center, fullerene-fullerene and phenyl-phenyl pairings averaged over the SAMSEN output states, their minimized states, and the MD end states, as well as the corresponding potential of mean force given by

$$U(r) = -k_b T \ln(g(r)) \tag{11}$$

In the center-to-center distributions of figure 6a (where the uniformly weighted geometrical average is taken as the center), the SAMSEN outputs show a slightly muted nearest and second nearest neighbor peak and a raised minimum between the two, when compared to the MD simulations. The system appears to have changed very little during energy minimization, as the radial distribution and potential of mean force are almost perfectly overlapping with the SAMSEN outputs.

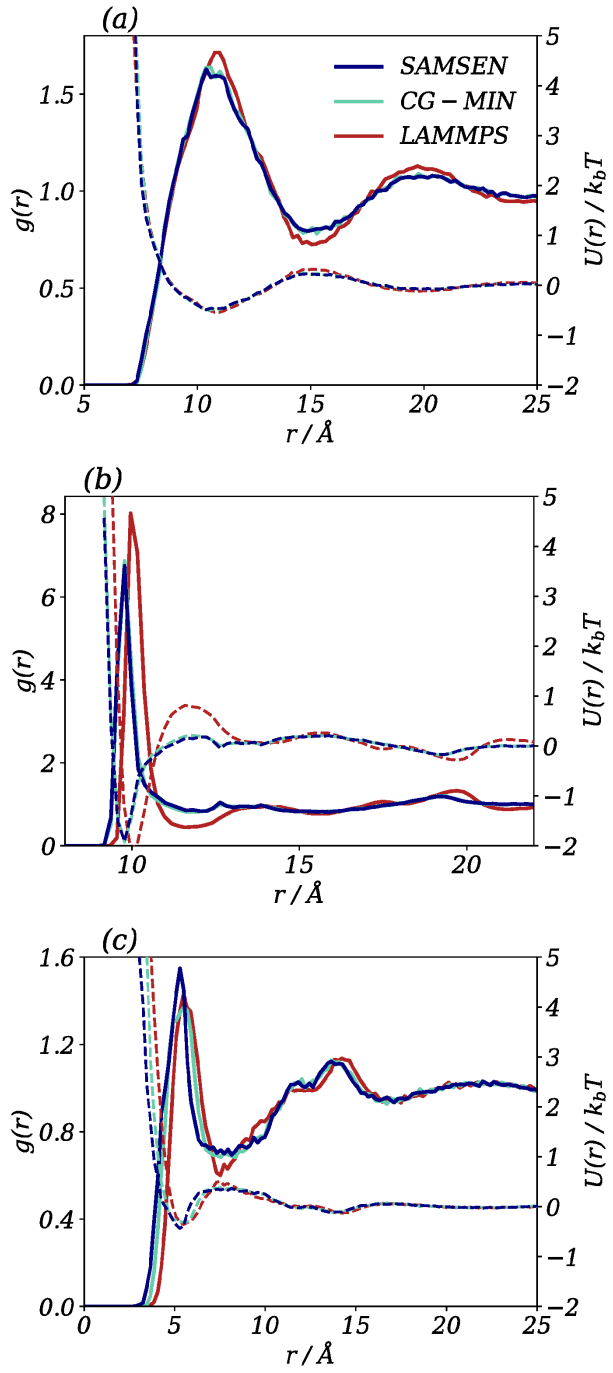

FIG. 6. The radial distribution functions (solid) and the corresponding potential of mean force (dotted) for (a) center-to-center, (b) fullerene-to-fullerene, and (c) phenyl-to-phenyl for the SAMSEN outputs, conjugant-gradient minimized states (CG-MIN) and final LAMMPS states for PCBM. Little change is observed between SAMSEN and minimized states (except in (c)). Additional detail is obtained after the MD simulation, recreating other studies. The $g(r)$ peaks also shift to larger separations.

The center-center results resemble that of a liquid and have similarities to the radial distribution of Neumann et al.[6], who were also attempting to reduce the computational burden of simulating morphologies. The simulation parameters of that study do, however, limit the usefulness of further comparison.

In figure 6b, the fullerene-fullerene $g(r)$ and corresponding $U(r)$ are shown. In $g(r)$ a sharp nearest neighbor peak attains an amplitude of nearly 7 for the SAMSEN outputs and minimized states. The minimization has again changed very little, while the MD nearest neighbour peak has shifted to higher separations (by about 0.2 Å) and broadens, with additional detail added to the first minima and subsequent peaks. The nearest-neighbor peak is slightly shallower than that of Cheung et al., both at an amplitude of just over 8. The remainder of the features in the MD radial distribution strongly resembles that of Cheung et al.[43] and Tummala et al.[10], capturing similar amplitudes and peak positions to simulations of an initially crystalline morphology and amorphous layer (in a polymer/bilayer morphology) respectively. As charge transport between PCBM molecules is predominantly between the fullerene sections[43], it is important that this short-range structure can be recreated if one was to then proceed and perform charge transport simulations using these morphologies. The largest difference is observed in $U(r)$ with an effective repulsive region at 12 Å strongly dampened in the SAMSEN outputs. This may be a consequence of simplifying the interactions. However, it may also be suggesting that SAMSEN is sampling states in a manner different to that which the calculation of $U(r)$ in equation 11 assumes - instead of being biased towards low energy configurations, SAMSEN may be sampling without such bias and applying MD then allows the equilibrium distribution of states to be sampled. At distances beyond the nearest neighbour peak, the SAMSEN $U(r)$ also appears generally softer than in the MD states. It is possible that structural differences such as increased penetration of atoms in the fullerene cage are dampening the effective potential.

The phenyl-to-phenyl radial distributions before and after the MD simulation are shown in figure 6c. The features of each of the distributions are similar in shape, with the SAMSEN peak being largest and reducing during minimization, but peaking somewhere in between the two and shifting to higher separations after MD. The $U(r)$'s are similar except the for the repulsive region at distances shorter than first nearest neighbour which starts at a smaller separations and has the lowest gradient for SAMSEN compared to both minimized and MD states. We attribute the differences in positions and detail in the $g(r)$ and $U(r)$ at short-range between SAMSEN and both the minimised and MD states to both the simplified external interactions and the treatment of PCBM

as a single rigid section (which as we have seen in the case of α–NPD can have a significant effect on structure).

Despite these differences the SAMSEN outputs have provided a reasonable first approximation to the MD simulated states, demonstrated by their proximity to the minimum and similarities in $U(r)$, perhaps suggesting that SAMSEN is sampling a similar free energy surface. The SAMSEN states can then be quickly minimized and equilibrated in MD, producing the expected structures and densities reliably. The SAMSEN and MD states were produced on a timescale much shorter than one would expect from an MD-only simulation, where undergoing structural relaxation is unfeasible below the PCBM glass transition temperature (118.3 to 131.2 °C depending on experimental method[48,49]).

IV. CONCLUSIONS

Using SAMSEN we have demonstrated how utilizing geometric simulation and following a series of low-frequency normal mode displacements allows multiple independent morphologies of organic semiconductor materials to be generated at amorphous thin film-density with modest computational resources.

By studying a system of buckminsterfullerenes, we showed the appearance of band-like vibrational frequencies starting at $\phi = 0.47$ (ellipsoid packing fraction of 1.12) and further splitting at higher densities. By displacing molecules along an equal number of the modes in each band we have shown that the lowest frequency band leads to computationally-faster structural relaxation. We also demonstrate how increasing the amplitude and the number of modes can lead to structural relaxation in less than two simulation cycles. This vastly reduces the required simulation time to generate a new output state of dense amorphous solids, where dynamic arrest prevents structural relaxation.

Turning to α–NPD, we show how varying the number of rigid sections alters the frequency spectrum, the relaxation time and the radial distribution function. Counterintuitively, the most coarse-grained simulation (the single rigid section α–NPD) produces the most detailed radial distribution function, which we attribute to more strongly constraining the molecular structure, but had the slowest relaxation time. Turning α–NPD into rigid sections using the procedure in section II A produced the fastest relaxation and compute times.

Treating PCBM as a single rigid body, SAMSEN produced a reasonable first approximation

to a realistic morphology, albeit with muted peaks in the radial distribution. Using molecular dynamics and an all-atom force-field[43], we are able to reliably recreate the longer-range structural details and peak amplitudes upon reaching $T = 300$ K and $P = 1$ atm, starting from the SAMSEN output. The short range structure was slightly altered during this process, which we attribute to a change in density and additional flexibility granted to the molecular structure.

By attempting to recreate the work of Cheung et al. and Tummala et al., we demonstrate that the generation of molecular morphologies can be performed quickly through structural relaxation and without access to high-performance computing facilities. This opens up the possibility of simulating even larger systems by reducing the length of time spent performing molecular dynamics simulations. For the presented results, all SAMSEN simulations were performed without parallelization on a desktop computer. With the correct choice of central frequency and mode calculation range, both eigenvalues and vectors can be solved for $N = 1000$ in less than 2 seconds when run on a single core. For the PCBM SAMSEN simulations, the time required to undergo structural relaxation using a single core was about 6 hours. If the SAMSEN parameters are chosen well —high amplitudes, low-frequency modes and an appropriate step resolution —simulations of more complex molecules could also be performed in short compute times.

Using SAMSEN to generate independent states (and using a short MD procedure to find an equilibrium structure) means that simulating material properties, where both nanoscale and mesoscale morphology matters, is much less computationally strenuous and larger system sizes and better statistics can be obtained. This will also help in the study of blends of materials, where it becomes important to sample many states, each with different mixing ratios and domain sizes. SAMSEN opens up the possibility of performing such studies entirely on a desktop PC if the MD equilibration procedure used here was refined. We also envisage SAMSEN being useful in the modelling of polymeric systems.

ACKNOWLEDGMENTS

The authors thank S. A. Wells and T. J. McManus for discussions on the FRODA algorithm and T. L. Underwood, C. Zannoni, O. Roscioni, M. Ricci and M. Allen for useful discussions.

Funding was received from the European Union Horizon 2020 Research and Innovation Programme under Grant Agreement 646176 and the Engineering and Physical Sciences Research Council's Centre for Doctoral Training in New and Sustainable Photovoltaics.

REFERENCES

[1]C. Groves, Reports on Progress in Physics **80**, 026502 (2017).

[2]B. Kumar, B. K. Kaushik, and Y. S. Negi, J. Mater. Sci. Mater. Electron. **25**, 1 (2014).

[3]H. Sirringhaus, Adv. Mater. **26**, 1319 (2014).

[4]K. Ding, X. Liu, and S. R. Forrest, Nano Lett. **18**, 3180 (2018).

[5]R. Noriega, J. Rivnay, K. Vandewal, F. P. V. Koch, N. Stingelin, P. Smith, M. F. Toney, and A. Salleo, Nat. Mater. **12**, 1038 (2013).

[6]T. Neumann, D. Danilov, C. Lennartz, and W. Wenzel, J. Comput. Chem. **34**, 2716 (2013).

[7]T. T. To and S. Adams, Phys. Chem. Chem. Phys. **16**, 4653 (2014).

[8]S. E. Root, S. Savagatrup, C. J. Pais, G. Arya, and D. J. Lipomi, Macromolecules **49**, 2886 (2016).

[9]M. L. Jones, D. M. Huang, B. Chakrabarti, and C. Groves, J. Phys. Chem. C **120**, 4240 (2016).

[10]N. R. Tummala, C. Bruner, C. Risko, J. L. Brédas, and R. H. Dauskardt, ACS Appl. Mater. Interfaces **7**, 9957 (2015).

[11]P. Friederich, V. Rodin, F. Von Wrochem, and W. Wenzel, ACS Appl. Mater. Interfaces **10**, 1881 (2018).

[12]M. L. Jones and E. Jankowski, Molecular Simulation **43**, 756 (2017).

[13]M. Lamarra, L. Muccioli, S. Orlandi, and C. Zannoni, Phys. Chem. Chem. Phys. **14**, 5368 (2012).

[14]D. M. Huang, R. Faller, K. Do, and A. J. Moule, J. Chem. Theory Comput. **6**, 526 (2010).

[15]S. E. Root, N. E. Jackson, S. Savagatrup, G. Arya, and D. J. Lipomi, Energy Environ. Sci. **10**, 558 (2017).

[16]M. Wyart, Ann. Phys. Fr. **30**, 1 (2005).

[17]I. Bahar, A. R. Atilgan, M. C. Demirel, and B. Erman, Phys. Rev. Lett. **80**, 2733 (1998).

[18]S. Wells, S. Menor, B. Hespenheide, and M. F. Thorpe, Phys. Biol. **2**, S127 (2005).

[19]B. Brooks and M. Karplus, Proc. Natl. Acad. Sci. U.S.A. **80**, 6571 (1983).

[20]A. R. Atilgan, S. R. Durell, R. L. Jernigan, M. C. Demirel, O. Keskin, and I. Bahar, Biophys. J. **80**, 505 (2001).

[21]J. E. Jimenez-Roldan, R. B. Freedman, R. A. Römer, and S. A. Wells, Phys. Biol. **9**, 016008 (2012).

[22]W. G. Krebs, V. Alexandrov, C. A. Wilson, N. Echols, H. Yu, and M. Gerstein, Proteins **48**, 682

(2002).

[23]E. Tjhung and T. Kawasaki, Soft Matter **13**, 111 (2017).

[24]K. Chen, M. L. Manning, P. J. Yunker, W. G. Ellenbroek, Z. Zhang, A. J. Liu, and A. G. Yodh, Phys. Rev. Lett. **107**, 1 (2011).

[25]M. M. Tirion, Phys. Rev. Lett. **77**, 1905 (1996).

[26]A. Widmer-Cooper, H. Perry, P. Harrowell, and D. R. Reichman, J. Chem. Phys. **131** (2009).

[27]D. J. Jacobs, A. J. Rader, L. A. Khun, and M. F. Thorpe, Proteins **44**, 150 (2001).

[28]S. Alfano and M. L. Greer, J. Guid. Control Dyn. **26**, 106 (2003).

[29]F. Gomes and D. Sorensen, *ARPACK++, a C++ implementation of ARPACK eigenvalue package* (Center for Research on Parallel Computation, Rice University, 1998).

[30]R. J. Boyd, J. Phys. B **10**, 2283 (1977).

[31]S. A. Wells and A. Sartbaeva, Mol. Simul. **41**, 1409 (2015).

[32]H. E. Pence and A. Williams, J. Chem. Educ. **87**, 1123 (2010).

[33]W. L. Jorgensen, D. S. Maxwell, and J. Tirado-Rives, J. Am. Chen. Soc. **118**, 11225 (1996).

[34]J. C. Maxwell, Philos. Mag. **27**, 294 (1864).

[35]E. Tjhung and L. Berthier, Phys. Rev. E **96**, 1 (2017).

[36]J.-P. Hansen and I. McDonald, *The Theory of Simple Liquids*, 3rd ed. (Academic Press, 2008).

[37]J. Horbach and W. Kob, Phys. Rev. E **64**, 14 (2001).

[38]C. S. O'Hern, L. E. Silbert, A. J. Liu, and S. R. Nagel, Phys. Rev. E **68**, 1 (2003).

[39]P. Friederich, F. Symalla, V. Meded, T. Neumann, and W. Wenzel, Journal of Chemical Theory and Computation **10**, 3720 (2014).

[40]F. Suzuki, S. Kubo, T. Fukushima, and H. Kaji, Sci. Rep. **8**, 1 (2018).

[41]A. Farahzadi, M. Beigmohamadi, P. Niyamakom, S. Kremers, N. Meyer, M. Heuken, and M. Wuttig, Appl. Surf. Sci. **256**, 6612 (2010).

[42]M. Shibata, Y. Sakai, and D. Yokoyama, J. Mater. Chem. C **3**, 11178 (2015).

[43]D. L. Cheung and A. Troisi, J. Chem. Phys. **114**, 20479 (2010).

[44]E. Polak and G. Ribérie, Rev. Fr. Inform. Rech. Oper. **16-R1**, 35 (1969).

[45]S. Plimpton, J. Comput. Phys. **117**, 1 (1995).

[46]S. Nosé, J. Chem. Phys. **81**, 511 (1984).

[47]W. Hoover, Phys. Rev. A **31**, 1695 (1985).

[48]J. Zhao, A. Swinnen, G. V. Assche, J. Manca, D. Vanderzande, and B. V. Mele, J. Phys. Chem. A **113**, 1587 (2009).

[49]T. T. Ngo, D. N. Nguyen, and V. T. Nguyen, Adv. Nat. Sci: Nanosci. Nanotechnol. **3**, 045001 (2012).